

# Unraveling the cause for the unusual processing behavior of commercial partially bio-based poly(butylene succinates) and their stabilization

Jannik Hallstein<sup>1</sup> | André Gomoll<sup>2</sup> | Antje Lieske<sup>2</sup> | Thomas Büsse<sup>2</sup> |  
Jens Balko<sup>2</sup> | Robert Brüll<sup>1</sup> | Frank Malz<sup>1</sup> | Elke Metzsch-Zilligen<sup>1</sup> |  
Rudolf Pfaendner<sup>1</sup> | Daniel Zehm<sup>2</sup> 

<sup>1</sup>Research Division Plastics, Fraunhofer Institute for Structural Durability and System Reliability LBF, Darmstadt, Germany

<sup>2</sup>Research Division Synthesis and Polymer Technology, Fraunhofer Institute for Applied Polymer Research IAP, Potsdam-Golm, Germany

## Correspondence

Rudolf Pfaendner, Fraunhofer Institute for Structural Durability and System Reliability LBF Schlossgartenstr. 6, 64289 Darmstadt, Germany.  
Email: rudolf.pfaendner@lbf.fraunhofer.de

Daniel Zehm, Fraunhofer Institute for Applied Polymer Research IAP  
Geiselbergstr. 69, 14476, Potsdam-Golm, Germany.  
Email: daniel.zehm@iap.fraunhofer.de

## Funding information

Fraunhofer-Gesellschaft

## Abstract

The commercially available partially bio-based poly(butylene succinate) (PBS) and poly(butylene succinate-co-adipate) (PBSA) are subjected to prolonged and multiple extrusion cycles to investigate their thermal behavior. Empirically, both PBS and PBSA form branches at 190°C, with PBS possessing a higher tendency for branching than PBSA as studied by rheology and size exclusion chromatography (SEC). In each case, the branching is favored by fumaric acid moieties, making both PBS and PBSA susceptible to accelerated thermal oxidation. Indeed, the NMR signal attributed to fumaric acid disappears upon thermal processing of PBS and PBSA. Presumably, the bio-based succinic acid used contains minor quantities of fumaric acid, yet still sufficient to cause this surprising processing behavior. The branching of both polymers is suppressed by stabilizers such as phenolic antioxidants, as proven by rheology and SEC. This is complemented by nuclear magnetic resonance (NMR), revealing that the fumaric acid signal is still well-resolved in the stabilized processed samples.

## KEYWORDS

polybutylene succinate, processing, rheology, stabilization, NMR, SEC

## 1 | INTRODUCTION

The increasing awareness of the consumer for the integration of sustainable economic strategies forces the plastics industry to provide answers that contribute in reducing environmental pollution and in optimizing solid-waste management. One answer to this complex social problem might be the use of bioplastics, which are polymers being either bio-based, biodegradable, or

both.<sup>1</sup> Apart from the bioplastic poly(lactic acid) (PLA), which is increasingly used in the market, poly(butylene succinate) (PBS), and poly(butylene succinate-co-adipate) (PBSA) are promising candidates with the potential to replace petro-based polymers. Both polymers are biodegradable and it has been shown that the rate of PBS to degrade in soil is higher than the rate of PLA,<sup>1,2</sup> which might be requested for certain applications. Further, although the monomers

This is an open access article under the terms of the Creative Commons Attribution-NonCommercial-NoDerivs License, which permits use and distribution in any medium, provided the original work is properly cited, the use is non-commercial and no modifications or adaptations are made.

© 2021 The Authors. *Journal of Applied Polymer Science* published by Wiley Periodicals LLC.

1,4-butanediol, succinic acid, and optionally adipic acid are currently mainly derived from fossil based resources, processes based on fermentation are established and become increasingly competitive.<sup>3,4</sup> For example, PTT MCC Biochem as most visible supplier produces and sells partially bio-based PBS since 2017 and the current total capacity worldwide is estimated at 25,000 tons/year.<sup>5</sup>

Current research activities are mainly devoted to develop PBS flexible film applications such as for packaging, mulch films, and composting bags.<sup>6</sup> This has also stimulated research intended to adjust the melt strength of PBS, which was achieved either by chain extension<sup>7–10</sup> or long-chain branching.<sup>11–14</sup> Further, the modification of PBS with itaconic and maleic acid by chain extension or copolymerization, respectively, is also described.<sup>15,16</sup> The subsequent treatment with benzoyl peroxide led to the formation of branched and cross-linked PBS, since the introduced unsaturated groups are sensitive to radical reactions. However, this strategy requires careful control of the peroxide addition and the processing conditions, because the formation of a cross-linked material is undesirably for film application.

Due to its high ductility, PBS is often used in combination with PLA to overcome the brittleness of PLA.<sup>17</sup> This can be done through conventional melt blending or by reactive extrusion of PLA and PBS using multifunctional additives.<sup>18–25</sup> Consequently, both strategies require process temperatures adjusted to the higher melting point of poly(L-lactic acid) (PLLA) ( $T_m \sim 175^\circ\text{C}$ ) compared to PBS ( $T_m \sim 115^\circ\text{C}$ ) and PBSA ( $T_m \sim 85^\circ\text{C}$ ). Similar temperature conditions are necessary for injection molding to ensure good melt flow. Therefore, PBS must withstand much higher thermal load in blends than pure PBS requires.

The detailed study of the thermal stability of polymers to establish processing conditions and service temperature is essential to guarantee a well-balanced property profile of the resulting applications. In the context of PBS, the few studies available suggest that the processing of linear PBS at  $190^\circ\text{C}$  leads to uncontrolled degradation reactions.<sup>26–28</sup> However, the described nature and effects of the degradation reactions are contradictory between the individual studies. Processing studies performed with Bionolle grades revealed a decrease of the molar mass as evidenced by reduced viscosities and gel permeation chromatography results, which was attributed to thermal oxidation and  $\beta$ -hydrogen transfer.<sup>26,28,29</sup> In contrast, Georgousopoulou et al. investigated the thermal stability of an PBS grade provided by Natureplast, reporting that the melt flow index (MFI) decreased after one extrusion,<sup>27</sup> which indicates a substantial increase of the molar mass after the first extrusion cycle. The authors attribute this to branching/recombination reactions, but neither the chain structure after the suggested

branching nor the mechanisms of such branching reactions, the occurrence of which is in clear contrast to other aliphatic polyesters such as PLA<sup>30</sup> or PHB,<sup>31</sup> are further investigated. Instead, they reported the processing stability effects by incorporating primary and secondary antioxidants again without clarifying the involved mechanisms.

The contradicting observations of the different groups obtained at the same processing temperature of  $190^\circ\text{C}$  are somewhat puzzling, considering that pure PBS was used in all cases. Moreover, the utility of these studies for practitioners is difficult to judge, since (i) the PBS material Bionolle provided by Showa Highpolymer Co., Ltd., is no longer available, and (ii) the source of the PBS from the distributor Natureplast is unknown. We do not know whether the effects the authors observed have generic significance, rather than being merely an unusual feature of the specific PBS materials used. Therefore, it is worth studying the next generation of commercial PBS grades, which will be used by practitioners and are provided by PTT MCC Biochem. Hence, the processing behavior of two available grades was investigated. Moreover, although  $T_m$  of PBS is about  $115^\circ\text{C}$ , the temperature selected for extrusion was  $190^\circ\text{C}$ , since these conditions reflect the processing of PLA/PBS blends. Furthermore, processing was correlated to rheological properties of the polymer melt as studied by oscillatory shear rheology and the molar mass to unveil chemical changes of the polymer. Finally, multiple extrusion was carried out using a twin screw-extruder to simulate multiple processing steps, for example, compounding and injection molding or mechanical recycling.

## 2 | EXPERIMENTAL SECTION

### 2.1 | Materials

In this work, commercially available poly(butylene succinate) (BioPBS™ FZ91PB) and poly(butylene succinate-co-adipate) (BioPBS™ FD92PM) were used. The PBS grade is an all-purpose grade suitable for film extrusion and injection molding. The PBSA grade is suitable for film extrusion. Both polymers were supplied by PTT MCC Biochem in the form of granules.

For the stabilization of both PBS and PBSA, primary and secondary antioxidants were used. Bis(2,4-dicumylphenyl) pentaerythritol diphosphite (Doverphos S-9228 (PS1)) was supplied by Dover Chemical. Butyric acid, 3,3-bis(3-tert-butyl-4-hydroxyphenyl)ethylene ester (Hostanox O3 (AO1)) was supplied by Clariant AG. A 1:1 mixture of tris(2,4-di-tert-butylphenyl)phosphite and pentaerythritol tetrakis[3-[3,5-di-tert-butyl-4-hydroxyphenyl]propionate (ADK STAB A-611 (AO2: PS2)) was supplied by Adeka Corporation.

## 2.2 | Processing: Micro compounder

Samples were prepared by compounding the polymer and the additives in a DSM Xplore 5cc twin-screw micro-compounder by Xplore Instruments BV (Sittard, NL). Therefore, the PBS and PBSA granules were milled and dried at 70°C overnight in a vacuum dryer to a moisture content of less than 100 ppm. Subsequently, the polymer (3 g) was mixed with the additives (6 mg, 0.2 wt%) and compounded at a set barrel temperature of 190°C and screw speed of 200 rpm for 5, 10, and 30 min respectively. Melt temperature at the die was measured to be ~185°C. During compounding, the vertical force was measured to evaluate possible change in melt properties weight of the polymer.

## 2.3 | Processing: Twin-screw extruder

Multiple extrusion cycles were performed on the co-rotating twin-screw extruder ZSE 27MAXX (Leistritz Extrusionstechnik GmbH, Nurnberg, Germany) at a speed of rotation  $n = 200 \text{ min}^{-1}$  with a throughput of 4–6 kg/h. For the barrels, an increasing temperature profile was set from 120°C in the feed zone to 160°C at the 5 mm nozzle. The single-strand was extruded from the nozzle at a melt temperature of ~170°C followed by cooling in a water bath, drying in compressed air and pelletizing. Prior to each extrusion cycle, the granules were stored in a dry-air dryer GTT 101 ES (Gerco, Warendorf/Germany) at a temperature of 70°C for 1 h to maintain a moisture content of less than 300 ppm. For the stabilized formulation the PBS granulate (6 kg) was premixed with the antioxidant PS1 (12 g, 0.2 wt%), followed by repeated extrusion cycles.

## 2.4 | Characterization

MFI measurements were done according to DIN EN ISO 1133 with the mflow device (Zwick/Roell) and a weight of 10 kg. About 5–10 g of the predried granules (70°C, 1 h) were heated at 190°C for 200 s. Mean value and standard deviation of three MFI measurements were determined, respectively.

Dynamic viscoelastic spectra were obtained with a ARES rheometer (TA Instruments). We used a parallel plate–plate geometry with a plate radius of 25 mm, separated by a gap of 650  $\mu\text{m}$ . The samples were loaded into the rheometer and equilibrated for 5 min at 130°C. Then, strain sweep experiments with strains ranging from 0.01% to 100% were performed at  $\omega = 10 \text{ rad/s}$  and 130°C in order to determine the linear viscoelastic regime.

Subsequently, dynamic frequency sweeps were conducted over a frequency range of 500–0.5 rad/s at 130°C with a strain of 0.5%.

$^1\text{H}$ -NMR samples were prepared by dissolving about 30 mg of the polymer in 0.6 ml  $\text{CDCl}_3$ . Solution  $^1\text{H}$  NMR spectra were recorded on a Varian Unity INOVA 500 NB spectrometer operating at 500 MHz spectra frequency. The proton-decoupled  $^{31}\text{P}$  melt-NMR spectra were acquired on a Varian Mercury-VX 400 nuclear magnetic resonance (NMR) spectrometer using a high-temperature 10 mm probe. About 2 g of each PBS samples was melted directly in a 10 mm NMR tube at 150°C. The  $^{31}\text{P}$  melt-NMR spectra (162 MHz spectra frequency) were recorded without lock (no solvent used) at 150°C.

Size exclusion chromatography (SEC) measurements were performed using SEC 1260 system by Agilent Technologies consisting of a degasser (G1322A), isocratic pump (G1310B), autosampler (G1329B), thermostat (G1316A), variable wavelength detector (G1314F), refractive index detector (G7800A), two Agilent-PLgel-MIXED-C columns and PLgel guard column. Chloroform was used as eluent ( $c = 2 \text{ g l}^{-1}$ ) at 35°C with a flow rate of  $1 \text{ ml min}^{-1}$ . Calibration was performed using polystyrene standard over a molecular weight distribution of 370–364.000  $\text{g mol}^{-1}$ .

## 3 | RESULTS AND DISCUSSION

During PBS/PLA extrusion studies using commercial PBS grades provided by PTT MCC Biochem at 190°C, which is required to process PLA, we sporadically observed an unusual increase in pressure during the extrusion, which became even more pronounced the higher the PBS content was and indicates that the melt viscosity was markedly increased. A search of the literature disclosed few references to the thermal stability of PBS.<sup>26–29</sup> In none of the references given above is mention made about effects that could explain our observations. Hence, efforts have been made to understand this rather surprising observation, which is presented here.

### 3.1 | Lab scale extrusion of commercial PBS and PBSA

To study the aforementioned observation in more detail, two commercial grades were selected, namely BioPBS™ FZ91PB and FD92PM, and compounded for 5, 10, and 30 min using a DSM Xplore 5cc twin-screw micro-compounder (200 rpm). While FZ91PB is PBS, the product FD92PM stands for a copolymer with about 20 mol% (with respect to the total acid units) of

adipic acid (PBSA). For the sake of brevity, we introduce the shorthand notation PBS-(X) and PBSA-(Y), where both X and Y are the extrusion time. The extrusion times of 5 and 10 min were selected to provide experimental conditions representing the combined processing duration of a material composed of both compounding and injection molding. The rather long treatment of 30 min was performed to simulate multiple processing cycles.

For the investigation of the processing behavior of both PBS and PBSA, the vertical force was continuously measured. The normalized vertical force is then plotted as a function of extrusion time, as exemplarily shown for both PBS-(30) and PBSA-(30) in Figure 1 (the samples compounded for 5 and 10 min are illustrated Figure S1). After a short period of plasticization, the force to process PBS-(X) progressively increases until a maximum is reached after about 10 min, where the measured force is about 80% higher than initially. If the thermal treatment of PBS-(X) is continued for 30 min the vertical force decreases, but did not reach the original level. The force acting is still 60% greater than initially measured. Less severe changes occurred to PBSA-(Y). Here, a maximum is reached after about 5 min, before the force decreases to the original level. Although the changes induced to PBSA-(Y) are at a lower level, the combined results constructed in Figure 1 imply that the viscosity of the polymer melts of both PBS-(X) and PBSA-(Y) increases during extrusion, leading to significantly higher vertical forces. It is probably worth emphasizing here that the

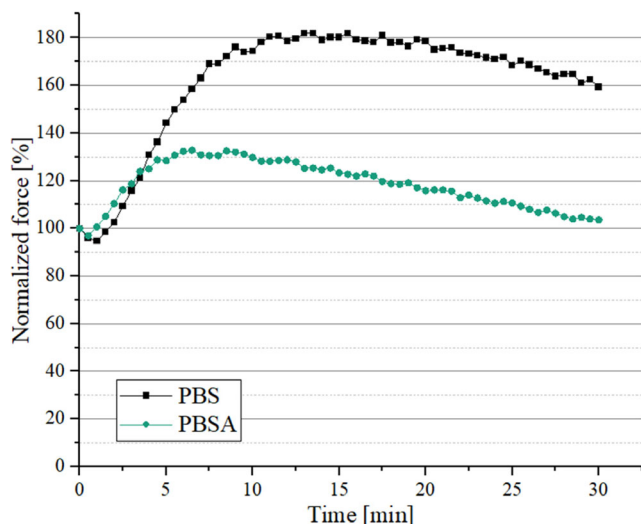


**FIGURE 1** Normalized vertical force during micro-compounding of PBS-(30) and PBSA-(30). The results obtained for the samples extruded for 5 and 10 min are not shown, for clarity of presentation. The curves are basically overlapping [Color figure can be viewed at [wileyonlinelibrary.com](http://wileyonlinelibrary.com)]

effects observed in previous investigations with the Bi-nolle grade would lead to a decrease in force, since these studies observed a decrease in molar mass.<sup>26–29</sup> Only the incidentally mentioned observation reported by Georgousopoulou et al. would correspond to our findings. However, the authors have not investigated this finding further.

The behavior of the PBS-(X) and PBSA-(Y) melts was further studied by oscillatory shear rheology, generating  $|\eta^*|$  (magnitude of complex viscosity),  $G'$  (storage, or elastic modulus), and  $G''$  (loss, or viscous modulus) as a

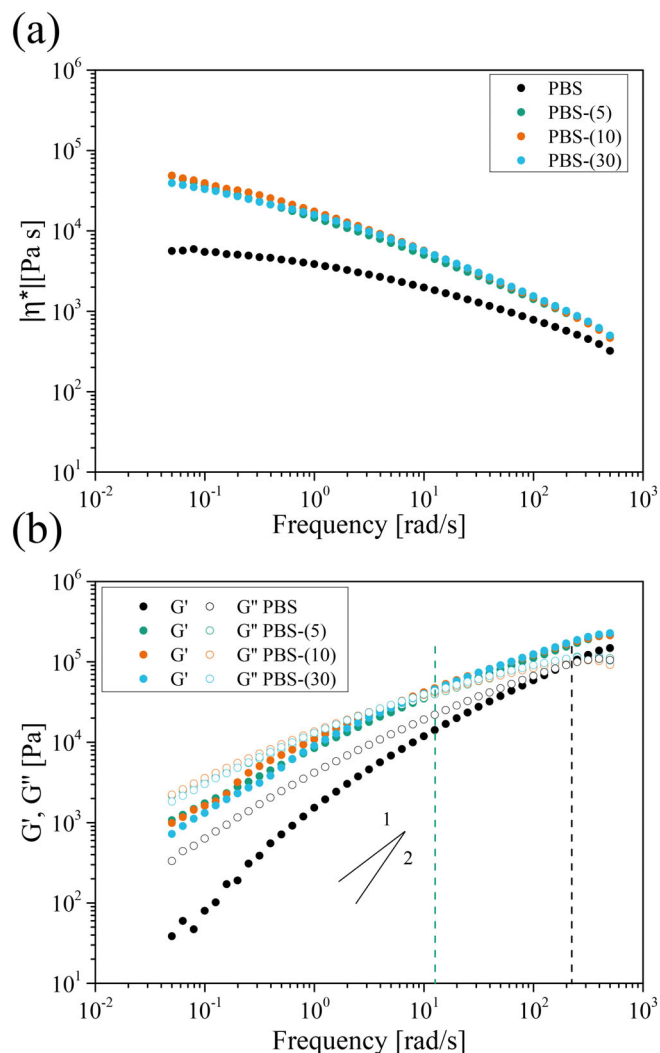


**FIGURE 2** Dynamic mechanical analysis of unprocessed PBS (black), PBS-(5) (green), PBS-(10) (orange), and PBS-(30) (blue) at 130°C, where (a) shows the frequency dependence of the complex viscosity  $|\eta^*|$ , and (b) the storage modulus ( $G'$ , closed cycles) and the loss modulus ( $G''$ , open cycles) as a function of the frequency  $\omega$ . The dashed black (for PBS) and green line (for PBS-(5)) refers to the crossover frequency  $\omega_{co}$ , at  $G'(\omega) = G''(\omega)$ , which can be converted to the relaxation time  $\lambda$  by  $1/\omega_{co}$ . The two lines representing the theoretical slopes of both  $G'(\omega)$  and  $G''(\omega)$  are used as guides for the eyes [Color figure can be viewed at [wileyonlinelibrary.com](http://wileyonlinelibrary.com)]

function of frequency  $\omega$  at a constant strain amplitude of  $\gamma = 0.5\%$ . Figure 2(a) shows the viscosity functions  $|\eta^*(\omega)|$  of both the unprocessed PBS and processed PBS-(X), which are clearly shifted to higher  $|\eta^*|$  in the low and high shear-rate regime. Further, the processed samples PBS-(5), PBS-(10), and PBS-(30) are significantly more shear-thinning, which is indicated by the shift of the onset of shear-thinning to lower  $\omega$  and the steeper slope in the power law region. A quantitative measure typically extracted from such viscosity functions  $|\eta^*(\omega)|$  is the zero shear-rate viscosity  $\eta_0$ , which is related to the melt strength of a polymer. However, unlike the unprocessed PBS, the strong non-Newtonian behavior of PBS-(5), PBS-(10), and PBS-(30) limits the analysis of the zero shear-rate viscosity  $\eta_0$  using the established Carreau–Yasuda model.<sup>32–34</sup> Hence, we determined the viscosity  $|\eta^*|_{0.1\text{rad/s}}$  at  $\omega = 0.1$  rad/s as a means to describe the melt strength: While  $|\eta^*|_{0.1\text{rad/s}}$  of PBS is about 5.780 Pa s, we estimated 36.900, 38.550, and 33.800 Pa s for PBS-(5), PBS-(10), and PBS-(30) (see Table 1). This significant increase of  $|\eta^*|_{0.1\text{rad/s}}$  reflects perfectly the results obtained during the force measurements as illustrated in Figure 1. Once a critical melt strength is reached, the investigated PBS degrades as the thermal treatment proceeds. This is illustrated by the decrease of  $|\eta^*|_{0.1\text{rad/s}}$  and the vertical force acting for PBS-(30).

While studying published data on linear PBS with increasing  $M_w$ ,<sup>35</sup> branched polyester such as PET or PBS, respectively,<sup>12,13,36–40</sup> and long-chain branched polyolefins<sup>41–49</sup> more carefully, we recognized that there are limitations in assigning the observations for the processed PBS-(X) to a single clear cause. In principle, higher viscosities and thus higher melt strength at low shear rates can be assigned to long-chain branches (LCB) or higher molar masses  $M_w$ , since both will enhance chain entanglements. The observed shear-thinning

**TABLE 1** Rheological characteristics (at 130°C) of both unprocessed and processed PBS and PBSA

Polymer	$ \eta^* _{0.1\text{rad/s}}$ <sup>a</sup> (Pa s)	Slope $G'$	Slope $G''$	$\lambda^b$ (s)
PBS	5780	1.4	0.8	0.005
PBS-(5)	36,900	0.7	0.6	0.085
PBS-(10)	38,550	0.9	0.6	0.18
PBS-(30)	33,800	0.8	0.7	0.1
PBSA	21,970	0.8	0.6	0.02
PBSA-(5)	38,130	0.8	0.6	0.11
PBSA-(10)	45,650	0.8	0.6	0.2
PBSA-(30)	25,710	0.9	0.4	0.12

<sup>a</sup>Complex viscosity at 0.1 rad/s.

<sup>b</sup>Relaxation time  $\lambda$  extracted from the crossover frequency  $\omega_{co}$ , at  $G'(\omega) = G''(\omega)$  using  $1/\omega_{co}$ .

behavior at higher shear rates can also be related to LCB, since they can easier disentangle due to their smaller hydrodynamic volumes than their linear counterparts, but the effects of the polydispersity  $\mathcal{D}$  will point in the same direction. This refers to a central problem in the rheological characterization of polymer melts, which is the separation of the effects induced by  $M_w$ ,  $\mathcal{D}$  and LCB.<sup>42,50</sup> We therefore assume that the  $M_w$  of the processed sample PBS-(5), PBS-(10), and PBS-(30) was increased by introducing branches during extrusion, which also leads to a higher  $\mathcal{D}$ . This view is supported by SEC analysis illustrated in Figure 3, which clearly reveals a shoulder at higher molar masses for PBS-(5), PBS-(10), and PBS-(30) (see also Table S1 for SEC results).

The formation of cross-linked materials is also likely to occur during extrusion if branching exceeds a certain degree. To exclude that cross-linking did occur, we carried out (i) solubility tests, which revealed that PBS-(5), PBS-(10), and PBS-(30) remained soluble in  $\text{CHCl}_3$ , and did (ii) strain sweep experiments, which are presented in Figure S3. Although these plots show that the ratio of  $G'(\gamma)$  and  $G''(\gamma)$  became smaller for PBS-(5), PBS-(10), and PBS-(30) (the curves of  $G'(\gamma)$  and  $G''(\gamma)$  are nearly overlapping), indicating that the elasticity of the materials increased, they do not show the characteristic behavior for cross-linked materials, which would lead to  $G'(\gamma) > G''(\gamma)$ .

The chain extension or branching for PBS-(5), PBS-(10), and PBS-(30) is further revealed by  $G'(\omega)$  and  $G''(\omega)$ . Figure 2(b) shows a typical set of both  $G'(\omega)$  and  $G''(\omega)$ , which are shifted to higher modulus for PBS-(5), PBS-(10), and PBS-(30). Moreover, while for PBS  $G'(\omega)$  and  $G''$

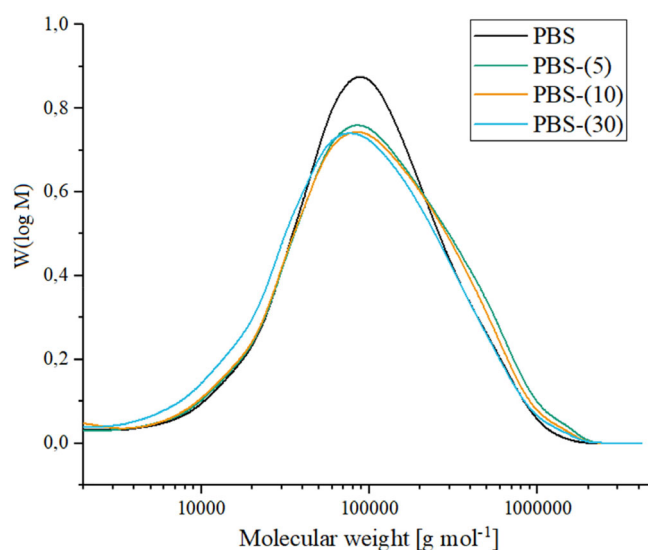


**FIGURE 3** Size exclusion chromatography (calibrated using PS standards) of neat and processed PBS in  $\text{CHCl}_3$  [Color figure can be viewed at wileyonlinelibrary.com]

( $\omega$ ) increasingly diverge in the low  $\omega$  region, nearly parallel curves of  $G'(\omega)$  and  $G''(\omega)$  were observed for PBS-(5), PBS-(10), and PBS-(30) below the crossover frequency  $\omega_{co}$ . This verbal description of  $G'(\omega)$  and  $G''(\omega)$  is also reflected by the slope of the curves in the terminal region at lower frequencies ( $\omega < 0.5$  rad/s), which we calculated for unprocessed PBS and PBS-(5), PBS-(10), and PBS-(30) and present in Table 1. The calculated slopes for PBS-(5), PBS-(10), and PBS-(30) are considerably lower than the theory suggests for linear polymers of narrow  $M_w$  distribution, where  $G'(\omega)$  and  $G''(\omega)$  are expected to be expressed by a power law of  $G'(\omega) \propto \omega^2$  and  $G''(\omega) \propto \omega$ .<sup>51</sup> The lower slopes of  $G'(\omega)$  and  $G''(\omega)$ , which are about 0.8 and 0.9 for PBS-(5), PBS-(10), and PBS-(30), and the higher absolute values of the dynamic moduli  $G'(\omega)$  and  $G''(\omega)$  clearly indicate the increasing elasticity of the materials, which agrees well with studies on branched polyester<sup>13</sup> and LCB polyolefins<sup>44</sup> and might be attributed to enhanced chain entanglements. Surprisingly, even the slopes of  $G'(\omega)$  and  $G''(\omega)$  for unprocessed PBS are also only 1.4 and 0.9, respectively (an explanation for this is given at the end of this section).

The incorporation of branching points also extends the long-term stability of the polymer melt drastically. A single branch point blocks several relaxation modes and shifts the relaxation spectrum by decades.<sup>34,40,52</sup> Inspecting  $G'(\omega)$  and  $G''(\omega)$  in Figure 2(b) in more detail, it becomes obvious that the crossover frequency  $\omega_{co}$ , (at  $G'(\omega) = G''(\omega)$ ), which converts to the relaxation time  $\lambda$  by  $1/\omega_{co}$ ,<sup>51</sup> is significantly shifted to lower frequencies. While  $\lambda$  of PBS is about of 0.005 s, we calculated 0.085, 0.18, and 0.1 s for PBS-(5), PBS-(10), and PBS-(30) for the longest relaxation mode, which are about two decades greater than  $\lambda$  of unprocessed PBS. The high impact of branching on the melt flow lies in their ability to form additional entanglements that restricts the reptation motion of a linear polymer chain.<sup>34,52,53</sup> The relaxation is inhibited until all branches/arms have freed themselves by arm retraction. Further, according to the tube model, the arms must be integrated as part of the polymer backbone, a process giving rise to much longer relaxation time than for linear chains. The new structure now resembles a linear chain, which continues to relax by reptation, but in a wider, diluted tube.

The study of the melt flow behavior of PBSA revealed significant differences. Figure 4(a) shows the viscosity functions  $|\eta^*(\omega)|$  of both the unprocessed PBSA and processed PBSA-(X), which are less strongly shifted to higher  $|\eta^*|$  in the frequency range investigated. Since the missing Newtonian plateau in the low shear-rate regime did not provide reliable results with the Carreau–Yasuda

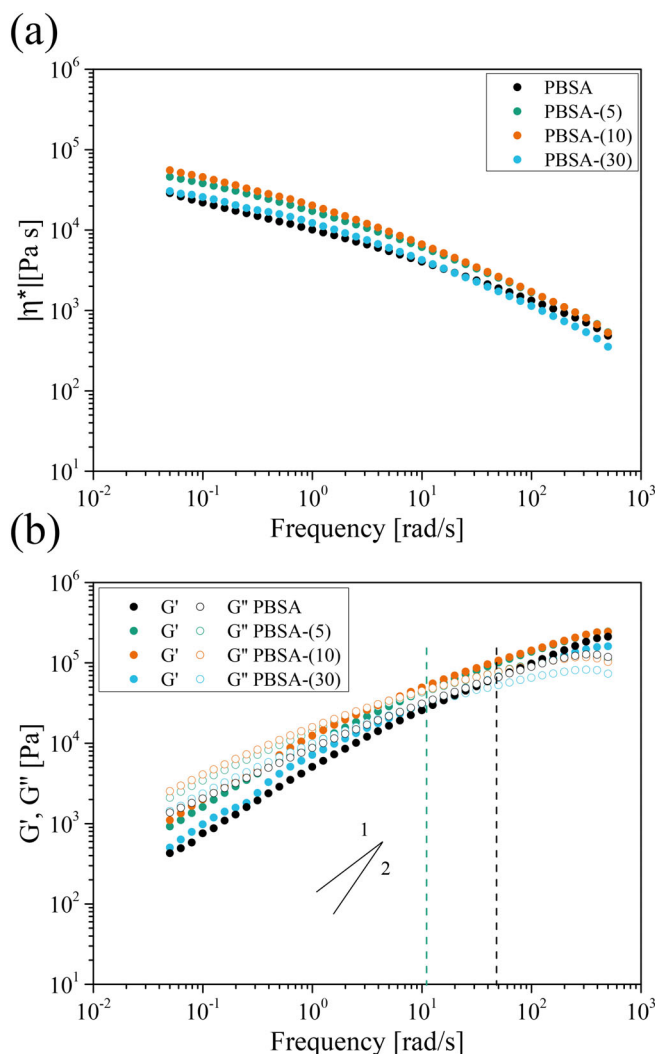


**FIGURE 4** Dynamic mechanical analysis of unprocessed PBSA (black), PBSA-(5) (green), PBSA-(10) (orange), and PBSA-(30) (blue) at 130°C, where (a) shows the frequency dependence of the complex viscosity  $|\eta^*|$ , and (b) the storage modulus ( $G'$ , closed circles) and the loss modulus ( $G''$ , open circles) as a function of the frequency  $\omega$ . The dashed black (for PBSA) and green line (for PBSA-(5)) refers to the crossover frequency  $\omega_{co}$ , at  $G'(\omega) = G''(\omega)$ , which can be converted to the relaxation time  $\lambda$  by  $1/\omega_{co}$ . The two lines representing the theoretical slopes of both  $G'(\omega)$  and  $G''(\omega)$  are used as guides for the eyes [Color figure can be viewed at [wileyonlinelibrary.com](http://wileyonlinelibrary.com)]

model, we used again  $|\eta^*|_{0.1 \text{ rad/s}}$  at  $\omega = 0.1$  rad/s to describe the melt strength. The estimation led to about 21.970 Pa s for PBSA and 38.130, 45.650, and 25.710 Pa s for PBSA-(5), PBSA-(10), and PBSA-(30) (see Table 1). This trend matches the results obtained during extrusion as illustrated in Figure 1, with  $|\eta^*(\omega)|$  of PBSA and PBSA-(30) being nearly overlapping. Further, unlike PBS, the melt of unprocessed PBSA possesses more pronounced shear-thinning behavior, with no significant difference being observed for PBSA-(5), PBSA-(10), and PBSA-(30).

Whether this observation can be related to different entanglement densities for both polymers or to the higher molar mass of PBSA (see Table S1) remains unclear at the moment, since the critical molar mass of entanglement  $M_c$  for PBSA is unknown, and the determination by using the well-known relationship  $\eta_0 \propto M_w^\alpha$ <sup>34,35,42,43,53,54</sup> is clearly out of the scope of the present investigation. Finally, solubility tests also revealed that no cross-linked material was formed.

The moderate shift to higher melt strength is also evident in  $G'(\omega)$  and  $G''(\omega)$  for PBSA-(5), PBSA-(10), and PBSA-(30) (see Figure 4(b)), indicating that the used PBSA is less sensitive to thermally induced structural changes than PBS. This is further reflected by SEC analysis, as shown in Figure 5, and by the crossover frequency  $\omega_{co}$  and the slopes of  $G'(\omega)$  and  $G''(\omega)$ , which are documented in Table 1. However, the combined results of PBS and PBSA show that the used PBSA inherently possesses a different relaxation behavior. This is evidenced by two observations: The longest relaxation time  $\lambda$ , calculated using the crossover frequency  $\omega_{co}$ , was found to be about 0.02 s for unprocessed PBSA, which is a decade slower than for unprocessed PBS. The slopes of  $G'(\omega)$  and  $G''(\omega)$  of PBSA were found to be 0.8 and 0.6, which are lower than for PBS and might again imply that PBSA possesses a different entanglement density than unprocessed PBS.

Finally, some additional comments are, perhaps, necessary with regard to the deviating slopes of  $G'(\omega)$  and  $G''(\omega)$  for both unprocessed PBS and PBSA from the theory for linear polymers with narrow  $\mathcal{D}$ . Such deviations are typically observed for branched polymers.<sup>13,40,44</sup> Further,

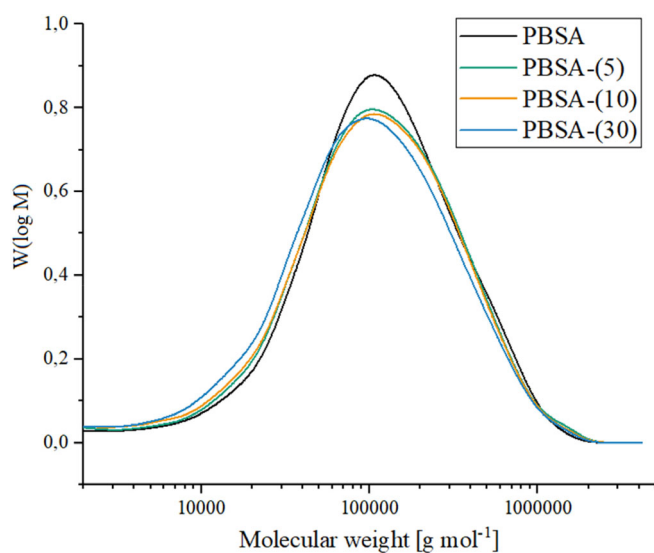


**FIGURE 5** Size exclusion chromatography (calibrated using PS standards) of neat and processed PBSA in  $\text{CHCl}_3$  [Color figure can be viewed at [wileyonlinelibrary.com](http://wileyonlinelibrary.com)]

when plotting the phase angle  $\delta$  versus magnitude of the complex modulus  $|G^*|$  (van Gorp-Palmen plot, vGP), linear polymers show an increase with a pronounced curvature with decreasing  $|G^*|$ , with  $\delta$  typically approaching  $90^\circ$ .<sup>33,34,55,56</sup> By contrast, PBS and PBSA do possess a significantly different shape, as shown in Figure 6. Here, a flattening is observed, with  $\delta$  approaching lower values than the theoretical  $90^\circ$ . The deviations increase with increasing the extrusion time, and are consistent with previous studies, indicating that higher degrees of branching cause more elastic behavior and shift the vGP curves to lower  $\delta$ . Hence, based on the combined data presented in this section, we assume that the commercial PBS and PBSA are also already slightly branched.

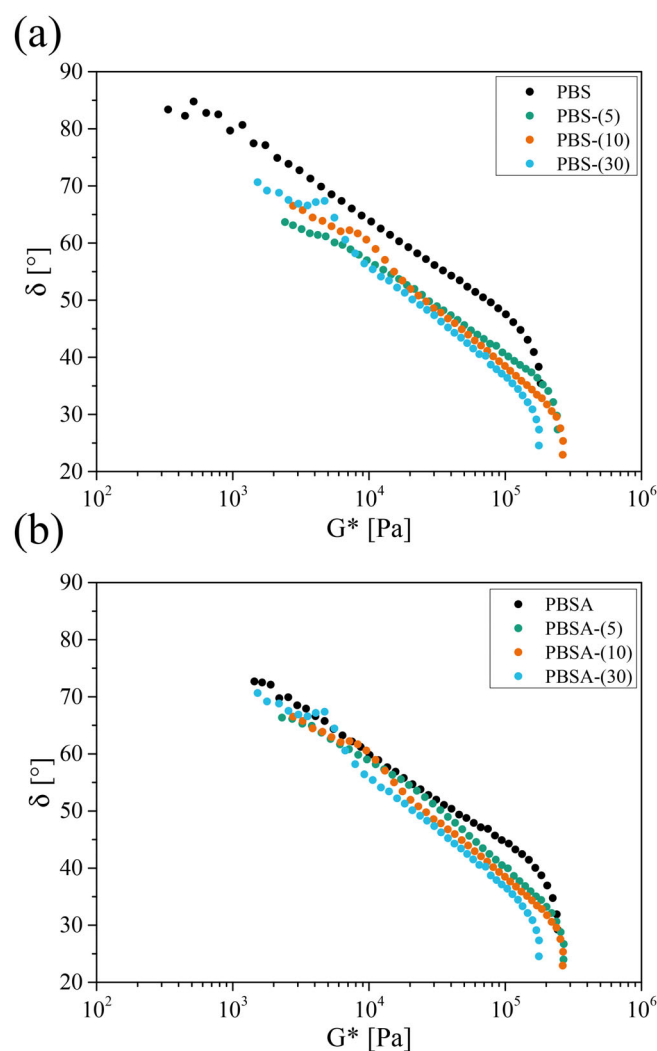


**FIGURE 6** Van Gorp-Palmen plot of neat and processed PBS and PBSA. (a) shows the phase angle  $\delta$  as the function of the complex modulus  $|G^*|$  of PBS (black), PBSA-(5) (green), PBSA-(10) (orange), while in (b) PBSA (black), PBSA-(5) (green), PBSA-(10) (orange), and PBSA-(30) (blue) are illustrated [Color figure can be viewed at [wileyonlinelibrary.com](http://wileyonlinelibrary.com)]

### 3.2 | Proposed branching mechanism

Having elucidated that the current commercial PBS and PBSA generation tends to form branches during extrusion at 190°C even without the addition of peroxides, it is pertinent to ask how the branching can occur. Based on the molecular structure of PBS and PBSA neither of them should form easily branched structures according to the three main decomposition modes known for polyesters (see Figure 7),<sup>57,58</sup> especially not within few minutes during extrusion as previous studies suggests.<sup>26–29</sup> Here, a decrease of the molar mass during processing was initially observed, which was either induced by hydrolysis or intramolecular  $\beta$ -H-transfer, respectively. By contrast, the thermal sensitivity of polyethylene to oxidation relies on vinyl, trans-vinylene, and vinylidene groups formed during the polymerization, which are already present in the as-obtained polymer and considerably susceptible to radicals generated during processing.<sup>59–62</sup>

Inspired by the thermal behavior of polyethylene, <sup>1</sup>H NMR investigations on commercial PBS and PBSA were performed. Figure 8 illustrates the <sup>1</sup>H NMR of both unprocessed PBS and PBSA recorded in deuterated chloroform (CDCl<sub>3</sub>). The chemical shifts observed for the hydrogens of PBS appear at 4.1, 2.6, and 1.7 ppm, while adipic acid in PBSA gives rise to additional resonances at 2.3 and 1.6 ppm. More importantly, the <sup>1</sup>H NMR of both spectra clearly reveal a well-resolved singlet at 6.8 ppm, which can unequivocally be assigned to the protons of fumaric acid.<sup>63,64</sup> Thus, we assume that the commercial PBS and PBSA contain vinylene groups resulting from the copolymerization of minor amounts of fumaric acid. This observation pleasantly surprised us and provides a logic to explain the processing behavior and the deviation

of the melt flow from linear polymers. As for the vinylene groups of polyethylene, the fumaric moieties are highly sensitive to oxygen and carbon-centered radicals, leading to long-chain branched PBS with a significantly higher melt strength as shown in Figure 2. This is supported by <sup>1</sup>H NMR spectra recorded for both PBS-(10) and PBSA-(10), which clearly show that the singlet at 6.8 ppm disappeared after processing (see Figure 8(f),(g)). Moreover, the vinylene groups introduced during the preparation of PBS by melt condensation may also react with nucleophiles such as 1,4-butanediol (BDO), which has become known in literature as Ordelt reaction and is particularly important in the field of unsaturated polyester resins.<sup>65–67</sup>

The addition of BDO forms a branching point that can grow further during the polycondensation, which leads to branched PBS and PBSA with the deviating melt flow behavior from linear polymers (see Figures 2 and 4). From studies on LCB polyethylene and polypropylene it is known that already low amounts of branching can cause such drastic effects in melt strength.<sup>41,42,47</sup>

One may of course question the origin of the fumaric acid in the final product. Although the patents currently held by Mitsubishi Chemicals describe also PBS examples containing minor amounts of malic acid,<sup>68</sup> which is supposed to eliminate thermally H<sub>2</sub>O to yield fumaric acid (and maleic acid), it remains uncertain whether malic acid has intentionally been added. However, as claimed in the patent, the used succinic acid, which is an intermediate of the tricarboxylic acid cycle (TCA cycle),<sup>69</sup> is received by fermentation using the oxidative TCA pathway (aerobic conditions). This process requires strategies to minimize the conversion of succinate to fumarate by inactivation of the *sdhA* gene (succinate dehydrogenase).<sup>70</sup> If this conversion is not blocked efficiently, traces

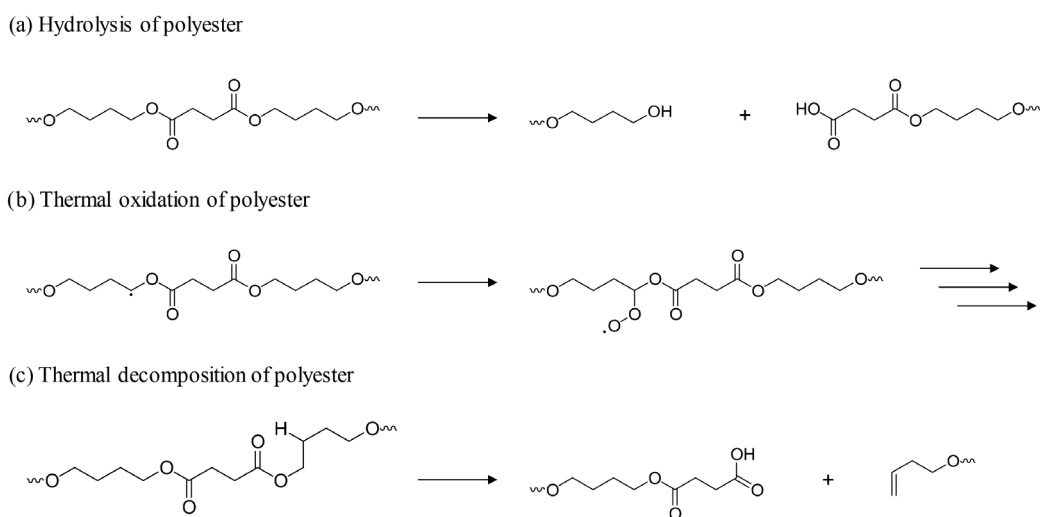
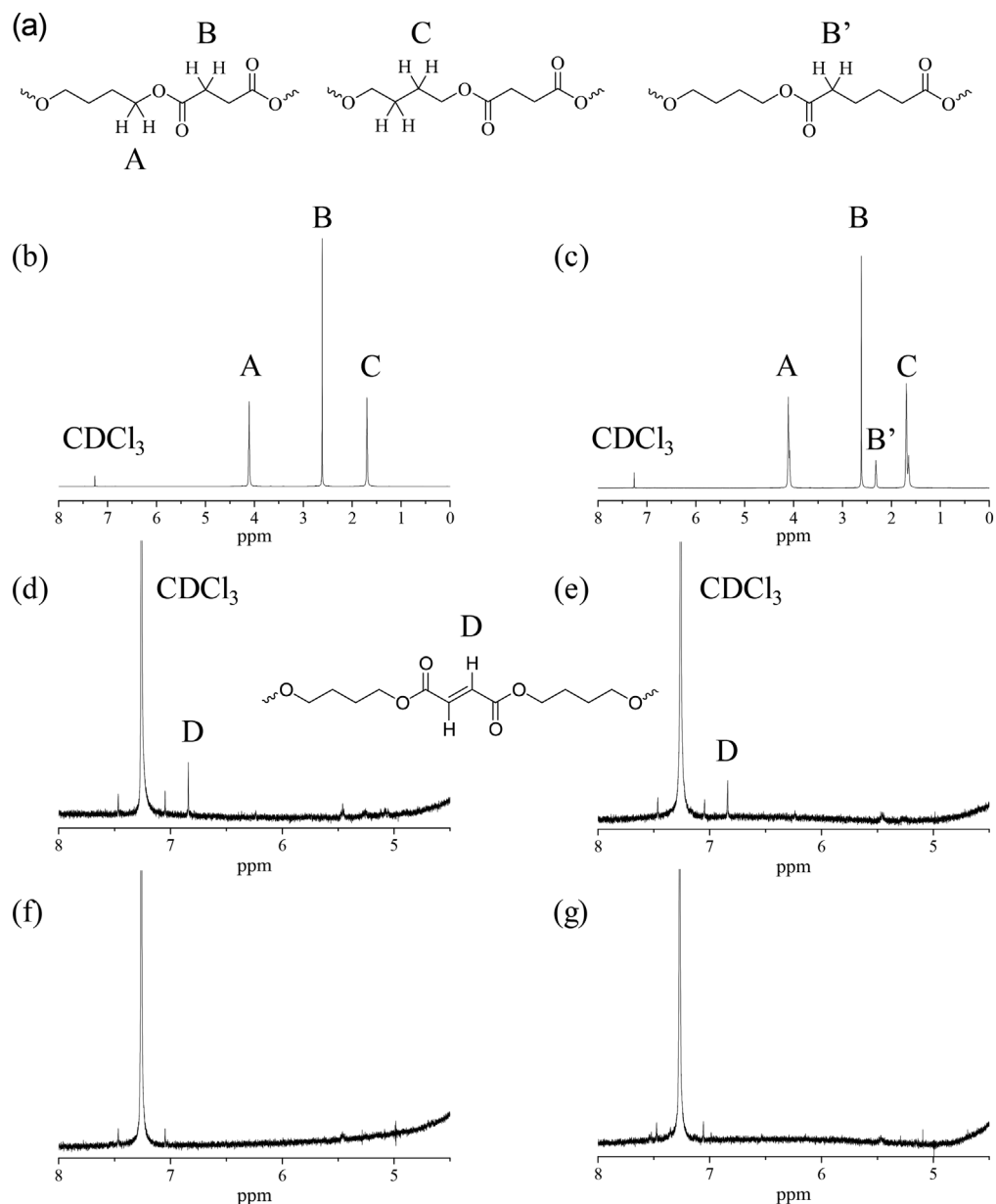


**FIGURE 7** Summary of the well-known degradation reactions of polyester, which are: Hydrolysis (a), thermal oxidation (b), and thermal degradation of polyester (c). For the sake of clarity, the degradation reactions have been transferred to PBS

**FIGURE 8**  $^1\text{H}$  NMR spectra (500 MHz, in  $\text{CDCl}_3$ ) recorded for (b) PBS and (c) PBSA, with the structural assignment illustrated in (a). The expansion of the 4.5–8 ppm region for (d) PBS and (e) PBSA is also shown, indicating the appearance of a well-resolved singlet at 6.8 ppm. This well-resolved singlet can unequivocally be assigned to the protons of fumaric acid, which disappear after the extrusion as indicated by spectra recorded for (f) PBS-(10) and (g) PBSA-(10)



of fumaric acid might remain in the final product that cause the above mentioned effects. This also explains the lower sensitivity of PBSA during processing, since PBSA contains fewer succinic acid and hence less fumaric acid is incorporated.

### 3.3 | Stabilization of PBS and PBSA

As described in the previous section the commercial PBS and PBSA are highly sensitive to thermooxidative degradation. To achieve process stabilization phenolic antioxidants (AO) and phosphite antioxidants (PS) were added (see Section 2), which are shown in Figure 9. PBS and PBSA were stabilized by adding 0.2 wt% of PS1, AO1 and

a 1:1 mixture of AO2 and PS2. Figure 10 exemplarily displays the normalized vertical force for the stabilized PBS and PBSA compounded for 30 min (the samples compounded for 5 and 10 min are illustrated Figure S2). After a slight decrease in vertical force during the first 2–3 min of compounding, which can be attributed to melt homogenization and transesterification during the initial phase of the compounding process, the force maintained at a constant level, indicating neither chain branching nor chain scission induced during compounding. This conclusion is supported by SEC analysis illustrated in Figure S11, which clearly shows that the chromatograms for the stabilized PBS and PBSA are perfectly overlapping. To our delight,  $^1\text{H}$  NMR investigations of both PBS-(0.2PS1-10) and PBSA-(0.2PS1-10) clearly reveal a

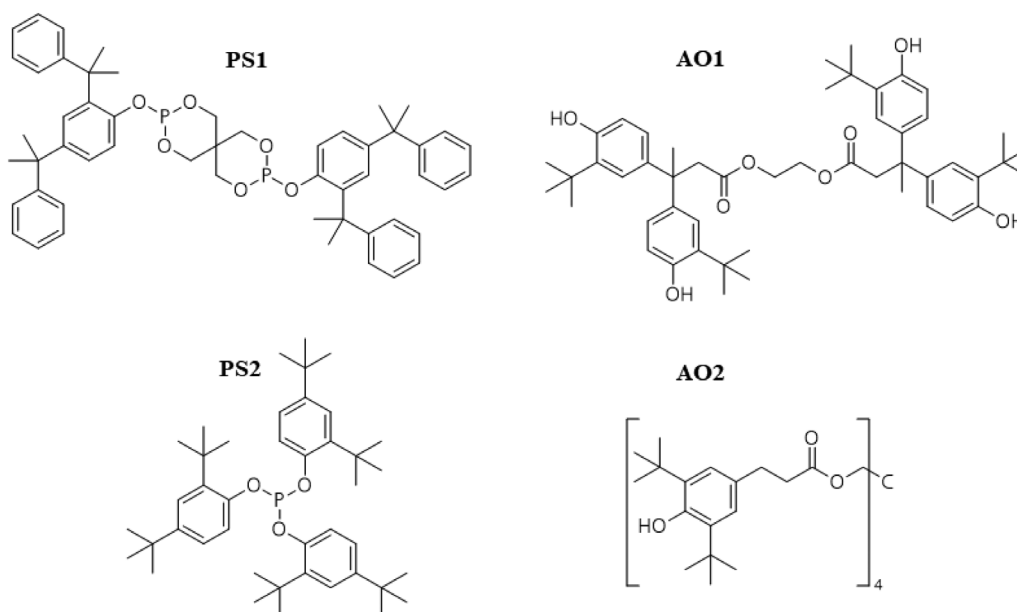


**FIGURE 9** Chemical structures of the used processing stabilizers

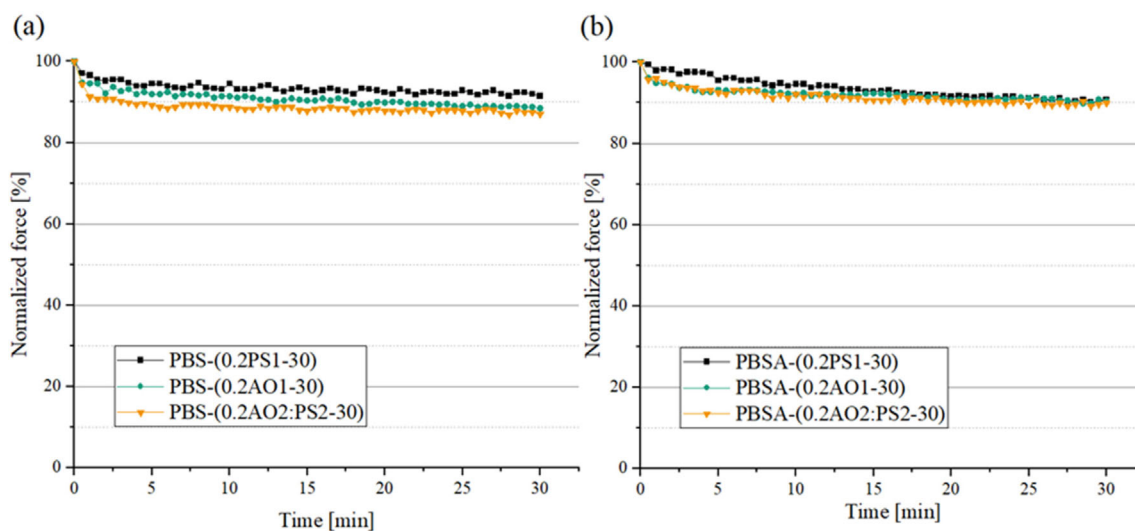


**FIGURE 10** Normalized vertical force measured during micro-compounding of stabilized PBS (a) and PBSA (b). The results obtained for the samples extruded for 5 and 10 min are not shown, for clarity of presentation. The curves are basically overlapping [Color figure can be viewed at [wileyonlinelibrary.com](http://wileyonlinelibrary.com)]

singlet at 6.8 ppm (see Figure S5 and S6). Hence, it can be concluded that the addition of the stabilizers clearly inhibits the radical branching reactions induced at the fumaric acid units as well as further thermal degradation reactions. More specifically, AO1 as a sterically hindered phenolic primary antioxidant acts as proton donor and inhibits the reaction between polymer radicals and the double bond. The secondary antioxidant PS1 is a phosphite stabilizer, which reacts with alkoxy- and peroxyradicals. Such radicals are formed due to the presence of oxygen and are effectively trapped by PS1. The

third stabilizer used is a combination of a sterically hindered phenol and a phosphite, which combines both stabilizing effects.<sup>57</sup>

The behavior of the PBS-(X) and PBSA-(Y) melts stabilized with AO1, PS1, and AO2:PS2 was further studied by oscillatory shear rheology. Figure 11 exemplarily shows the viscosity functions  $|\eta^*(\omega)|$  of PBS-(X) and PBSA-(Y) melts stabilized with PS1, which are nearly overlapping in the investigated  $\omega$  regime (see Figure S7–10 for both PBS and PBSA stabilized with AO1 and AO2:PS2). This is further reflected by the viscosity

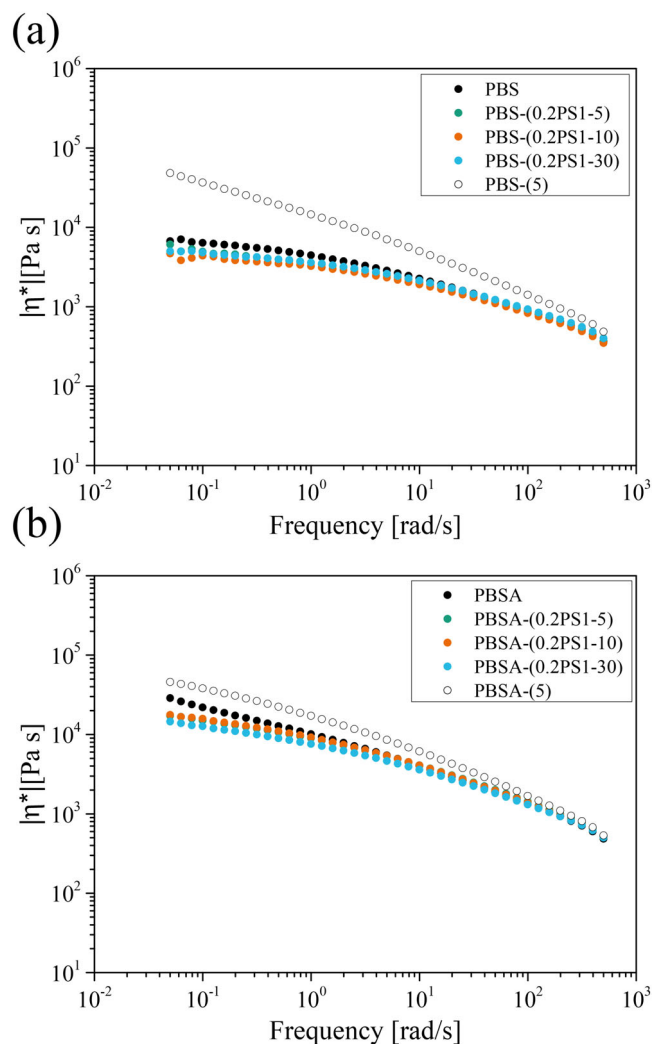


**FIGURE 11** Dynamic mechanical analysis at 130°C, where (a) shows the frequency dependence of the complex viscosity  $|\eta^*|$  for neat PBS (black), PBS-(0.2PS1-5) (green), PBS-(0.2PS1-10) (orange), and PBS-(0.2PS1-30) (blue), and (b) the complex viscosity  $|\eta^*|$  for neat PBSA (black), PBA-(0.2PS1-5) (green), PBA-(0.2PS1-10) (orange), and PBA-(0.2PS1-30) (blue). The curves represented by open cycles correspond to the unstabilized and extruded samples PBS-(5) and PBA-(5) [Color figure can be viewed at [wileyonlinelibrary.com](http://wileyonlinelibrary.com)]

$|\eta^*|_{0.1\text{rad/s}}$  at  $\omega = 0.1$  rad/s: While  $|\eta^*|_{0.1\text{rad/s}}$  of PBS is about 5.780 Pa s, we estimated 36.800 Pa s for PBS-(5), and about 4.900, 4.400, and 4.800 Pa s for PBS-(PS1-5), PBS-(PS1-10), and PBS-(PS1-30), which clearly demonstrates the stabilizing effect of PS1. Similar behavior was observed for PBA: While  $|\eta^*|_{0.1\text{rad/s}}$  of PBA is about 22.000 Pa s, we estimated 38.100 Pa s for PBA-(5), and about 15.000, 15.800, and 12.700 Pa s for PBA-(PS1-5), PBA-(PS1-10), and PBA-(PS1-30). The slight deviations observed for  $|\eta^*|_{0.1\text{rad/s}}$  of both PBS and PBA could be due to the low sensitivity of the instrument in the low-shear regime.

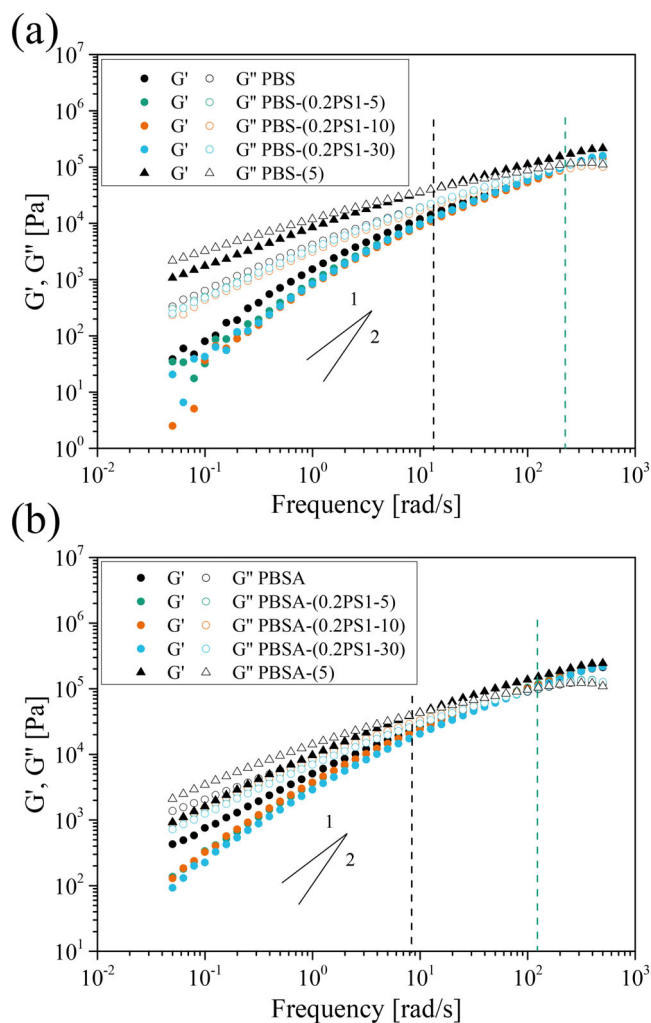


**FIGURE 12** Dynamic mechanical analysis at 130°C, where (a) shows the frequency dependence of the storage modulus ( $G'$ , closed cycles) and the loss modulus ( $G''$ , open cycles) as a function of the frequency  $\omega$  for neat PBS (black), PBS-(0.2PS1-5) (green), PBS-(0.2PS1-10) (orange), and PBS-(0.2PS1-30) (blue), and (b) the storage modulus ( $G'$ , closed cycles) and the loss modulus ( $G''$ , open cycles) as a function of the frequency  $\omega$  neat PBA (black), PBA-(0.2PS1-5) (green), PBA-(0.2PS1-10) (orange), and PBA-(0.2PS1-30) (blue). The curves represented by triangles correspond to the unstabilized and extruded samples PBS-(5) and PBA-(5) [Color figure can be viewed at [wileyonlinelibrary.com](http://wileyonlinelibrary.com)]

The stabilizing effect is further reflected by  $G'(\omega)$  and  $G''(\omega)$ . Figure 12 a shows a typical set of both  $G'(\omega)$  and  $G''(\omega)$  for PBS, which overlap for PBS-(PS1-5), PBS-(PS1-10), and PBS-(PS1-30). They start to scatter in the low  $\omega$  regime, which is due to the instrument becoming less sensitive when approaching 10 Pa s. Similarly, PBA-(PS1-5), PBA-(PS1-10), and PBA-(PS1-30) also perfectly overlap (see Figure 12(b)). However, two further observations are perhaps worth noting: First, the stabilized samples of both PBS and PBA are slightly shifted to lower  $G'$  and  $G''$  in the low  $\omega$  region. This implies that the stabilized

PBS and PBSA slightly degrade by transesterification or hydrolysis, respectively, during extrusion. Secondly, the slopes of  $G'(\omega)$  and  $G''(\omega)$  in the terminal region for the stabilized samples do not significantly differ from the neat sample. For example: While we found about 1.4 and 0.8 for PBS, the estimation of PBS-(PS1-5), PBS-(PS1-10), and PBS-(PS1-30) reveals 1.6 and 0.9. Similarly: the slopes of PBSA are 0.8 and 0.6, while 1.1 and 0.8 was observed for PBSA-(PS1-5), PBSA-(PS1-10), and PBSA-(PS1-30). This again implies that the neat PBS and PBSA are already slightly branched polymers, as discussed in Section 2.2.

It is generally assumed that the high stabilizing effect of additives is related to their good distribution in the polymer matrix. This certainly requires that the stabilizer dissolves in the polymer during processing. Otherwise, agglomeration is likely to occur, leading to poorly stabilized polymers. We exemplarily tested this assumption on PBS processed with PS1 using high temperature  $^{31}\text{P}$  liquid state NMR measured at  $150^\circ\text{C}$ , taking advantage that liquid state NMR spectroscopy only shows signals from liquids, gels and melts (nuclei of solids cannot be detected). The  $^{31}\text{P}$  melt NMR spectra (no solvent used) of both PBS processed at  $150^\circ\text{C}$  (Figure 13(a)) and  $190^\circ\text{C}$  (Figure 13(b)) with PS1 reveal a well resolved singlet at about 117 ppm. This signal can unequivocally be assigned to the  $^{31}\text{P}$  resonance of PS1, for which we recorded a reference spectra in  $\text{CDCl}_3$  (see Figure 13(c)). Therefore, the appearance of signal at 117 ppm clearly indicates that the stabilizer (PS1) dissolves in the polymer matrix. In contrast, the solid PS1 measured at  $150^\circ\text{C}$  – also without solvent – does not reveal any resonance

(Figure 13(d)) as expected. This is due to the fact that the melting point of PS1 at about  $225^\circ\text{C}$  is significantly higher than the measurement temperature and thus still exists as a solid in the NMR tube, in contrast to the melting states of the two PBS samples. Hence, it is perhaps plausible to assume that PS1 distributes well in PBS during processing to protect the polymer from molecular weight increase initiated through oxidation.

### 3.4 | Multiple extrusion cycles

In order to align the results obtained so far to industrial processing conditions, multiple extrusion cycles were carried out for PBS and PBS-(0.2PS1) using a co-rotating twin-screw extruder ZSE 27MAXX (see Section 2). PS1 was selected as processing stabilizer as it is one of the efficient phosphites with highest hydrolytic stability and sterically hindrance to avoid any other side reactions caused through byproducts from hydrolytic cleavage or transesterification. After each extrusion cycle the MFI was measured, the results are shown in Figure 14. As expected, the MFI of PBS significantly dropped by more than a factor of two after the first extrusion and even stronger by a factor of 20 after the second extrusion compared to 45 g/10 min for the granulate as delivered. It should be noted that the weight of 10 kg for the MFI measurements was chosen purposely to obtain MFI values covering the complete range of materials tested here. This reduction of MFI corresponds perfectly to the prominent rise of vertical force in micro-compounding of PBS during

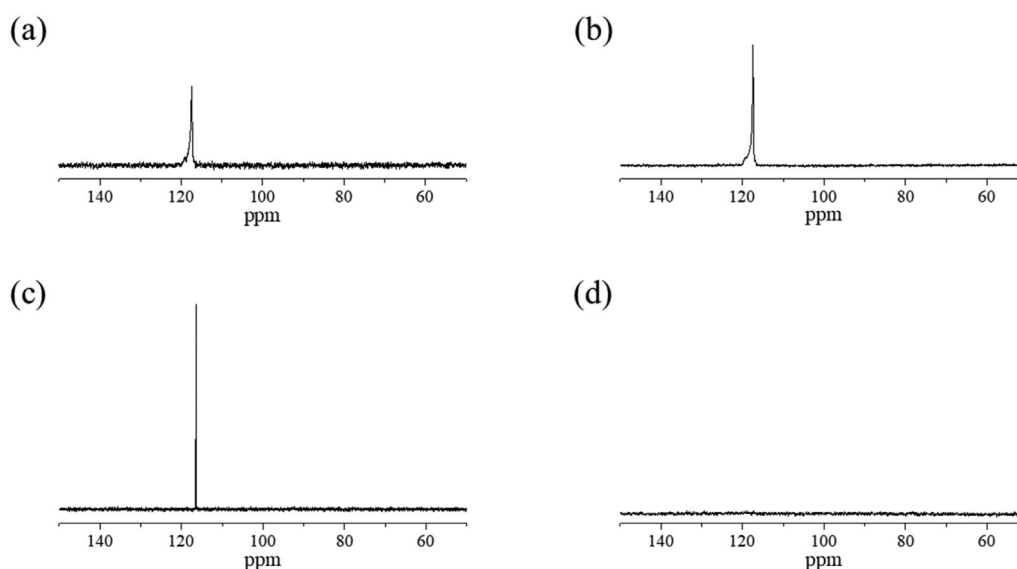


**FIGURE 13** High temperature  $^{31}\text{P}$  NMR spectra at  $150^\circ\text{C}$  (162 MHz) recorded for PBS processed at  $150^\circ\text{C}$  (a) and  $190^\circ\text{C}$  (b), both stabilized with PS1. The well-resolved singlet at about 117 ppm can be assigned to the phosphorus atom of PS1. For comparison, spectrum (c) shows the  $^{31}\text{P}$  NMR of PS1 recorded in  $\text{CDCl}_3$  and (d) of PS1 without a solvent recorded at  $150^\circ\text{C}$

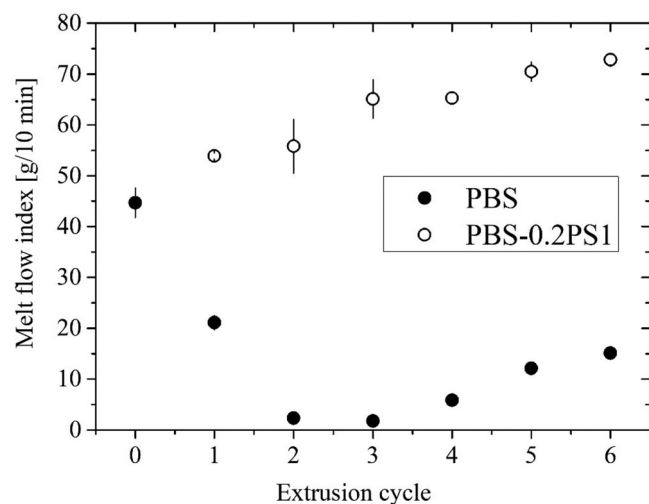


**FIGURE 14** Melt flow index (MFI) (190°C, 10 kg) after repeated processing on the co-rotating twin-screw extruder. Extrusion cycle 0 is the MFI for the granulate as delivered by the manufacturer

the first 10 min (Figure 1) and the increased melt viscosity from oscillatory shear measurements (Figure 2(a)). Using colored granulates, we estimated the mean residence time to about 3.5 min during an extrusion step. The lowest MFI value of 2.4 g/10 min is already obtained after the second extrusion step, implying that nearly complete thermo-mechanical branching is induced after about 7 min. For further repeated extrusion cycles ( $>3$ ) the MFI increases again, which can be attributed to the onset of molar mass reduction induced by chain scission.

It is perhaps worth emphasizing here that we observed similar effects using a co-rotating twin-screw extruder ZSE 27MAXX than using a micro-compounder, although the PBS melt temperature measured at the extruder nozzle was only 175°C, compared to 185°C measured during micro-compounding. This effect is further confirmed by rheological studies (see Figure 15(a)). As for the PBS series summarized in Figure 2 the viscosity functions  $|\eta^*(\omega)|$  are shifted to higher values, indicating the higher melt strength for the processed PBS in agreement with the measured MFI values. The branching for PBS-1E to PBS-6E is also reflected by  $G'(\omega)$  and  $G''(\omega)$ , which reveal higher absolute values as illustrated in Figure S12. The melt of PBS-3E was already difficult to measure due to the highly elastic and gel-like character ( $G'$  is greater than  $G''$  over the entire frequency range investigated), even though PBS-3E was still soluble in chloroform.

The PBS material compounded with PS1 completely differs in terms of melt properties after multiple extrusion steps. After the first extrusion the MFI of PBS-1E-(0.2PS1) is slightly higher than for the as-received, unstabilized PBS, that is, the addition of PS1 effectively suppresses the branching of PBS as intended (see

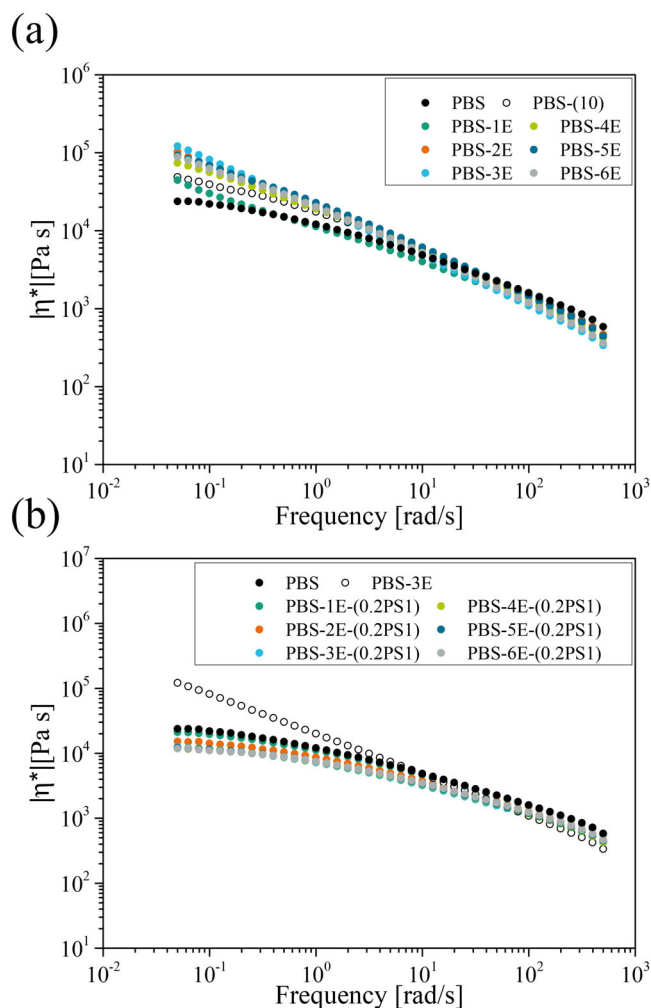


**FIGURE 15** Dynamic mechanical analysis at 130°C, where (a) shows the frequency dependence of the complex viscosity  $|\eta^*|$  for neat PBS (black), PBS-10 (black, open cycle) obtained using a micro-compounder, and PBS-1E (green), PBS-2E (orange), PBS-3E (light blue), PBS-4E (light green), PBS-5E (blue), and PBS-6E (gray) (blue). (b) Complex viscosity  $|\eta^*|$  as a function of frequency (at 130°C) shown for neat PBS (black), PBS-3E (black, open cycle) produced using a in twin-screw extruder, and the stabilized samples PBS-1E-(0.2PS1) (green), PBS-2E-(0.2PS1) (orange), PBS-3E-(0.2PS1) (light blue), PBS-4E-(0.2PS1) (light green), PBS-5E-(0.2PS1) (blue), and PBS-6E-(0.2PS1) (gray) (blue) [Color figure can be viewed at [wileyonlinelibrary.com](http://wileyonlinelibrary.com)]

Figure 14). This is also true for further repeated extrusion cycles ( $\geq 2$ ), with no decrease of the MFI being observed. Instead, the MFI continuously increases, indicating the decrease of the molar mass of PBS. This can be attributed to either hydrolysis induced by traces of H<sub>2</sub>O, which is more difficult to remove under industrial conditions, or to thermal decomposition by  $\beta$ -hydrogen transfer (see Figure 7). Since neither degradation reaction is based on a radical mechanism, the addition of the secondary antioxidant PS1 to prevent these aging phenomena is without any effect. The observed degradation also moderately

affects the melt flow behavior of the samples, as indicated by the slight shift of  $|\eta^*(\omega)|$  to lower values in the low frequency regime (see Figure 15(b)).

## 4 | CONCLUSION

Gaining knowledge about the thermal behavior of materials during processing is essential for both the fabrication of certain products and the selection of suitable additives to guarantee smooth and constant processing. However, the individual degradation modes are complicated and depend on the polymers considered. For polyesters such as PET, the main degradation reactions comprise hydrolysis, thermal oxidation by radicals generated through the combination of heat and mechanical stress, and thermal degradation by  $\beta$ -H-transfer leading to terminal vinyl groups, respectively. In contrast, the current bio-based PBS generation possesses some unique features, as the present study revealed. Unlike conventional polyesters, the bio-based PBS is susceptible to thermal oxidation via radical reactions. Therefore, PBS samples were thermally treated by prolonged heating and multiple extrusion cycles and investigated through rheology, SEC, and  $^1\text{H}$  NMR. Rheology and SEC suggest that the processing of partially bio-based PBS (and PBSA) leads to branching at  $190^\circ\text{C}$ , with the highest level of branching obtained after about 10 min. Moreover, the effects are more severe under industrial related conditions. Here, significant changes occurred already after the first extrusion cycle (3.5 min) and approached a maximum after the second cycle. This behavior can unequivocally be attributed to fumaric acid moieties incorporated into the PBS main chain, as detailed  $^1\text{H}$  NMR studies revealed. Moreover, the  $^1\text{H}$  NMR signal assigned to the fumaric acid is no longer appearing in the processed samples, implying that branching is induced at the fumaric acid moiety. All samples produced remained soluble in chloroform, which indicates that macroscopic cross-linking did not occur under the investigated conditions. By adding stabilizers such as phenolic and phosphite antioxidants the branching tendency is fully suppressed, whereas a well in the polymer matrix distributed high performance phosphite behaves best. Consequently, the  $^1\text{H}$  NMR signal of the fumaric acid moiety is still well-resolved. Hence, the antioxidants effectively trap radicals formed during the processing, preventing the branching of PBS by thermooxidative reaction modes. This behavior appears somehow similar to the thermooxidative degradation reactions of polyolefines, which contain vinyl, trans-vinylene, and vinylidene groups formed during the polymerization process.

However, having elucidated the cause for the processing sensitivity of the current bio-based PBS

generation, we would like to emphasize that the observed branching should not be treated as a problem. Instead, it should be viewed as a practical opportunity, which might offer potential for certain applications and further studies.

## ACKNOWLEDGMENTS

The authors acknowledge financial support by the Fraunhofer-Gesellschaft e.V., which supported this work as Fraunhofer Cluster of Excellence "Circular Plastics Economy." We also express our gratitude to the suppliers of polymers and additives for providing us with samples. We acknowledge H. Ziller, J. Kunkel and S. Böhler for technical assistance during multiple extrusion cycles and MFI measurements. Open Access funding enabled and organized by Projekt DEAL. WOA Institution: FRAUNHOFER-GESELLSCHAFT ZUR FORDERUNG DER ANGEWANDTEN FORSCHUNG EV Blended DEAL: Projekt DEAL

## CONFLICT OF INTEREST

The authors declare no competing financial interest.

## ORCID

Daniel Zehm  <https://orcid.org/0000-0003-2042-4356>

## REFERENCES

- [1] Y. Tokiwa, B. P. Calabia, C. U. Ugwu, S. Aiba, *Int. J. Mol. Sci.* **2009**, *10*, 3722.
- [2] M. Puchalski, G. Szparaga, T. Biela, A. Gutowska, S. Sztajnowski, I. Krucińska, *Polymer* **2018**, *10*, 251.
- [3] A. Burgard, M. J. Burk, R. Osterhout, S. van Dien, H. Yim, *Curr. Opin. Biotechnol.* **2016**, *42*, 118.
- [4] J. H. Ahn, Y.-S. Jang, S. Yup Lee, in *Industrial Biotechnology*, 1st ed. (Eds: C. Wittmann, J. C. Liao), Wiley-VCH Verlag GmbH & Co. KGaA, Weinheim **2017**, p. 505.
- [5] H. Käß, *Kunststoffe* **2019**, *10*, 134.
- [6] J. Xu, B.-H. Guo, in *Plastics from Bacteria*, 1st ed. (Ed: G. G.-Q. Chen), Springer Berlin Heidelberg, Berlin, Heidelberg **2010**, p. 347.
- [7] E. Takiyama, T. Fujimaki, in *Biodegradable Plastics and Polymers*, 1st ed. (Ed: K. F. Y. Doi), Elsevier, Amsterdam **1994**, p. 150.
- [8] V. Tserki, P. Matzinos, E. Pavlidou, C. Panayiotou, *Polym. Degrad. Stab.* **2006**, *91*, 377.
- [9] J. B. Zhao, K. Y. Li, W. T. Yang, *J. Appl. Polym. Sci.* **2007**, *106*, 590.
- [10] C. Q. Huang, S. Y. Luo, S. Y. Xu, J. B. Zhao, S. L. Jiang, W. T. Yang, *J. Appl. Polym. Sci.* **2010**, *115*, 1555.
- [11] G.-C. Liu, W.-Q. Zhang, S.-L. Zhou, X.-L. Wang, Y.-Z. Wang, *RSC Adv.* **2016**, *6*, 68942.
- [12] E. K. Kim, J. S. Bae, S. S. Im, B. C. Kim, Y. K. Han, *J. Appl. Polym. Sci.* **2001**, *80*, 1388.
- [13] G. Wang, B. Guo, R. Li, *J. Appl. Polym. Sci.* **2012**, *124*, 1271.
- [14] H. G. Chae, B. C. Kim, S. S. Im, Y. K. Han, *Polym. Eng. Sci.* **2001**, *41*, 1133.
- [15] H.-J. Jin, D.-S. Kim, B.-Y. Lee, M.-N. Kim, I.-M. Lee, H.-S. Lee, J.-S. Yoon, *J. Polym. Sci., Part B: Polym. Phys.* **2000**, *38*, 2240.

- [16] N. Teramoto, M. Ozeki, I. Fujiwara, M. Shibata, *J. Appl. Polym. Sci.* **2005**, *95*, 1473.
- [17] S. Su, R. Kopitzky, S. Tolga, S. Kabasci, *Polymer* **2019**, *11*, 1193.
- [18] J. W. Park, S. S. Im, *J. Appl. Polym. Sci.* **2002**, *86*, 647.
- [19] T. Yokohara, M. Yamaguchi, *Eur. Polym. J.* **2008**, *44*, 677.
- [20] M. Harada, T. Ohya, K. Iida, H. Hayashi, K. Hirano, H. Fukuda, *J. Appl. Polym. Sci.* **2007**, *106*, 1813.
- [21] R. Wang, S. Wang, Y. Zhang, C. Wan, P. Ma, *Polym. Eng. Sci.* **2009**, *49*, 26.
- [22] P. Chaiwutthinan, T. Leejarkpai, D. P. Kashima, S. Chuayjuljit, *Adv. Mater. Res.* **2013**, *664*, 644.
- [23] D. Ji, Z. Liu, X. Lan, F. Wu, B. Xie, M. Yang, *J. Appl. Polym. Sci.* **2014**, *131*, 39580.
- [24] X. Hu, T. Su, P. Li, Z. Wang, *Polym. Bull.* **2018**, *75*, 533.
- [25] M. Ma, L. Xu, K. Liu, S. Chen, H. He, Y. Shi, X. Wang, *J. Appl. Polym. Sci.* **2019**, *540*, 48646.
- [26] C. Kanemura, S. Nakashima, A. Hotta, *Polym. Degrad. Stab.* **2012**, *97*, 972.
- [27] I.-N. Georgousopoulou, S. Vouyiouka, P. Dole, C. D. Papaspyrides, *Polym. Degrad. Stab.* **2016**, *128*, 182.
- [28] K. Resch-Fauster, A. Klein, E. Blees, M. Feuchter, *Polym. Test.* **2017**, *64*, 287.
- [29] D. J. Kim, W. S. Kim, D. H. Lee, K. E. Min, L. S. Park, I. K. Kang, I. R. Jeon, K. H. Seo, *J. Appl. Polym. Sci.* **2001**, *81*, 1115.
- [30] N. S. Q. S. Amorin, G. Rosa, J. F. Alves, S. P. C. Gonçalves, S. M. M. Franchetti, G. J. M. Fechine, *J. Appl. Polym. Sci.* **2014**, *131*, 40023.
- [31] M. Zaverl, M. Ö. Seydibeyoğlu, M. Misra, A. Mohanty, *J. Appl. Polym. Sci.* **2012**, *125*, 324.
- [32] M. Gahleitner, *Prog. Polym. Sci.* **2001**, *26*, 895.
- [33] F. J. Stadler, H. Münstedt, *Macromol. Mater. Eng.* **2009**, *294*, 25.
- [34] P. Liu, W. Liu, W.-J. Wang, B.-G. Li, S. Zhu, *Macromol. React. Eng.* **2017**, *11*, 1600012.
- [35] M. Garin, L. Tighzert, I. Vroman, S. Marinkovic, B. Estrine, *J. Appl. Polym. Sci.* **2014**, *131*, 40887.
- [36] N. Hudson, W. A. MacDonald, A. Neilson, R. W. Richards, D. C. Sherrington, *Macromolecules* **2000**, *33*, 9255.
- [37] U. Yilmazer, M. Xanthos, G. Bayram, V. Tan, *J. Appl. Polym. Sci.* **2000**, *75*, 1371.
- [38] R. F. Rosu, R. A. Shanks, S. N. Bhattacharya, *Polym. Int.* **2000**, *49*, 203.
- [39] R. Dhavalikar, M. Yamaguchi, M. Xanthos, *J. Polym. Sci., Part A: Polym. Chem.* **2003**, *41*, 958.
- [40] M. Vandesteene, N. Jacquél, R. Saint-Loup, N. Boucard, C. Carrot, A. Rousseau, F. Fenouillot, *Chin. J. Polym. Sci.* **2016**, *34*, 873.
- [41] P. M. Wood-Adams, J. M. Dealy, A. W. de Groot, O. D. Redwine, *Macromolecules* **2000**, *33*, 7489.
- [42] A. Malmberg, C. Gabriel, T. Steffl, H. Münstedt, B. Löfgren, *Macromolecules* **2002**, *35*, 1038.
- [43] D. J. Lohse, S. T. Milner, L. J. Fetters, M. Xenidou, N. Hadjichristidis, R. A. Mendelson, C. A. García-Franco, M. K. Lyon, *Macromolecules* **2002**, *35*, 3066.
- [44] Z. Ye, F. AlObaidi, S. Zhu, *Macromol. Chem. Phys.* **2004**, *205*, 897.
- [45] W.-J. Wang, Z. Ye, H. Fan, B.-G. Li, S. Zhu, *Polymer* **2004**, *45*, 5497.
- [46] K. M. Kirkwood, L. G. Leal, D. Vlassopoulos, P. Driva, N. Hadjichristidis, *Macromolecules* **2009**, *42*, 9592.
- [47] Z. Ye, F. AlObaidi, S. Zhu, *Ind. Eng. Chem. Res.* **2004**, *43*, 2860.
- [48] M. Sugimoto, Y. Suzuki, K. Hyun, K. Hyun Ahn, T. Ushioda, A. Nishioka, T. Taniguchi, K. Koyama, *Rheol. Acta* **2006**, *46*, 33.
- [49] J. K. Jørgensen, K. Redford, E. Ommundsen, A. Stori, *J. Appl. Polym. Sci.* **2007**, *106*, 950.
- [50] S. G. Hatzikiriakos, *Polym. Eng. Sci.* **2000**, *40*, 2279.
- [51] T. G. Mezger, *Das Rheologie Handbuch*, 4th ed., Vincentz Network, Hannover **2012**, p. 163.
- [52] W. Pyckhout-Hintzen, J. Allgaier, D. Richter, *Eur. Polym. J.* **2011**, *47*, 474.
- [53] F. J. Stadler, *Rheol. Acta* **2012**, *51*, 821.
- [54] A. Pawlak, *Macromol. Chem. Phys.* **2019**, *220*, 1900043.
- [55] S. Trinkle, C. Friedrich, *Rheol. Acta* **2001**, *40*, 322.
- [56] S. Trinkle, P. Walter, C. Friedrich, *Rheol. Acta* **2002**, *41*, 103.
- [57] K. Schwarzenbach, B. Gilg, D. Müller, G. Knobloch, J.-R. Pauquet, P. Rota-Graziosi, A. Schmitter, J. Zingg, E. Kramer, in *Plastics Additives Handbook*, 6th ed. (Eds: H. Zweifel, R.-D. Maier, M. Schiller), Hanser, München **2009**, p. 1.
- [58] T. Rieckmann, S. Völker, in *Modern Polyesters: Chemistry and Technology of Polyesters and Copolyesters*, 1st ed. (Eds: J. Scheirs, T. E. Long), John Wiley & Sons, Ltd, Chichester **2004**, p. 29.
- [59] L. A. Pinheiro, M. A. Chinelatto, S. V. Canevarolo, *Polym. Degrad. Stab.* **2004**, *86*, 445.
- [60] R. Scaffaro, F. P. La Mantia, L. Botta, M. Morreale, N. Tz, P. M. Dintcheva, *Polym. Eng. Sci.* **2009**, *49*, 1316.
- [61] V. H. Rolón-Garrido, M. H. Wagner, *Polym. Degrad. Stab.* **2014**, *99*, 136.
- [62] A. A. Cuadri, J. E. Martín-Alfonso, *Polym. Degrad. Stab.* **2017**, *141*, 11.
- [63] M. Paci, V. Crescenzi, N. Supino, F. Campana, *Makromol. Chem.* **1982**, *183*, 377.
- [64] H. Sugitabi, M. Fukusawa, Y. Mukoyama, K. Isogai, *Anal. Sci.* **1992**, *8*, 637.
- [65] V. Z. Ordelt, *Makromol. Chem.* **1963**, *63*, 153.
- [66] A. Fradet, E. Marechal, *Makromol. Chem.* **1982**, *183*, 319.
- [67] Y. S. Yang, J. P. Pascault, *J. Appl. Polym. Sci.* **1997**, *64*, 133.
- [68] T. Aoshima, T. Hoshino, T. Uyeda, Y. Miki, (Mitsubishi Chemical Co.). EP 1640397 B1, 13.04.2016.
- [69] J. M. Berg, J. L. Tymoczko, L. Stryer, G. J. Gatto, *Biochemie*, 8th ed., Springer Spektrum, Berlin, Heidelberg **2018**, p. 581.
- [70] K.-K. Cheng, G.-Y. Wang, J. Zeng, J.-A. Zhang, *Biomed Res. Int.* **2013**, *2013*, 538790.

## SUPPORTING INFORMATION

Additional supporting information may be found online in the Supporting Information section at the end of this article.

**How to cite this article:** Hallstein J, Gomoll A, Lieske A, et al. Unraveling the cause for the unusual processing behavior of commercial partially bio-based poly(butylene succinates) and their stabilization. *J Appl Polym Sci.* 2021;e50669. <https://doi.org/10.1002/app.50669>